Journal of Sound and Vibration 329 (2010) 3537–3549

Contents lists available at ScienceDirect

Journal of Sound and Vibration

journal homepage: www.elsevier.com/locate/jsvi

The onset of friction-induced vibration and spragging

Jaeyoung Kang [a,*], Charles M. Krousgrill [b]

[a] Division of Mechanical and Automotive Engineering, Cheonan-Si, Kongju National University, Korea
[b] School of Mechanical Engineering, 585 Purdue Mall, Purdue University, West Lafayette, IN 47907-2088, USA

ARTICLE INFO

Article history:
Received 21 August 2009
Received in revised form
7 January 2010
Accepted 3 March 2010
Handling Editor: H. Ouyang
Available online 26 March 2010

ABSTRACT

The minimal dynamic models are used to investigate the influences of geometric coupling on frictionally-excited system. At a certain set of system parameters, spragging can occur where the steady-sliding is indeterminate. It is found that the sprag condition becomes the boundary of the regime for the non-existence of the equilibrium in the parametric space. Equilibrium instability induced by the negative friction-velocity slope and mode-coupling is determined for the regime in which the steady-sliding is defined. Its ensuing nonlinear response is shown to reach the stick-slip limit cycle.

1. Introduction

Self-excited vibration induced by friction has generated annoying noise in many applications such as brakes and mechanical gear systems. The mechanisms of friction-induced vibrations have been investigated for several decades: sprag-slip, negative friction-slope and mode-coupling, as reviewed in [1]. The negative friction-slope with respect to the sliding speed was widely applied to the friction-engaged system as a source of dynamic instability and its nonlinear behavior was characterized as limit cycle oscillations in [2–4].

On the other hand, the mode-coupling instability has been shown to be the source of the friction-induced vibration in systems with axi-symmetric components such as rotors and drums of automotive braking systems [5,6]. The flutter instability and its limit cycle response have been investigated for the case of coexistence of mode-coupling and negative friction-slope mechanisms [7–10].

In contrast, the sprag-slip mechanism has not been clearly explained in the current literature. This issue was actively studied as a possible source of brake squeal noise by many researchers through the 1970s. Spurr [11] determined a geometric condition for the appearance of unbounded contact forces, which is also referred to as the kinematic (or geometric) constrained instability. It was assumed by Spurr that for this instability "friction force is much increased above the value it would have in a perfectly rigid system. The assembly deflects elastically, reducing the frictional force and returns to its first state to repeat the cycle". This scenario is termed "sprag-slip oscillation". Jarvis and Mills [12] used a cantilevered beam on disc to examine sprag-slip instabilities in braking systems. The simple pin-disc model by Earles et al. [13] showed the necessary condition for instability in terms of the contact orientation. However, the interest on the sprag mechanism has diminished since 1980s when the mode-coupling mechanism gained acceptance as being a dominating factor in the production of brake squeal oscillations. Yet interest in sprag oscillations remain today in many applications.

Recently, the sprag-slip phenomena in the beam-on-belt configuration were re-examined in [14,15] focusing on the condition where a steady-sliding state does not exist. However, it is a more complicated model than a spring-block model that is typically used in the study of self-excited oscillation. It is relevant to study the simpler sprag models in order to make clear the dynamic response characteristics near the sprag condition. It is noted that the sprag model resembles

* Corresponding author.
E-mail addresses: jkang@kongju.ac.kr (J. Kang), krousgri@ecn.purdue.edu (C.M. Krousgrill).

0022-460X/$ - see front matter © 2010 Elsevier Ltd. All rights reserved.
doi:10.1016/j.jsv.2010.03.002

Painleve's problem [16,17] which describes the rigid-body with the Coulomb law of friction to penetrate the rigid surface at the certain conditions. This inconsistent condition is closely related to the sprag condition.

In the current paper, we develop simple friction-coupled models with spragging forces by using a mass on a traveling belt in both one- and two-dimensional spaces. The static and dynamic stability boundaries are provided in terms of the closed-form solutions. The onset of the equilibrium instability and the sprag condition for non-existence of steady-sliding response are determined through analytical and numerical procedures. In the last section, nonlinear examples are provided for showing the ensuing dynamic behavior of the equilibrium instability.

2. Derivation of the equations of motion

2.1. One-dimensional sprag model

The dynamic model of Spurr [11] is refined here in this study. Consider a rigid body hinged at point 'O' in Fig. 1(a), with the other end in contact with a surface moving at a constant speed $V(\neq 0)$. The body is pressed by a pre-load L, generating a normal contact force N and a friction force $F(=\mu N)$ on the rigid contact surface. For steady-sliding, a force and moment balance on the rigid body results in:

$$\frac{N}{L}=\frac{1}{1-\mu\tan\theta_o}, \tag{1}$$

From Eq. (1), it is seen that the contact force becomes infinite when

$$\mu=\frac{1}{\tan\theta_o}. \tag{2}$$

This is called the sprag condition subject to the geometric rigid model constraint.

It should be noted that the normal contact force N becomes negative if $1-\mu\tan\theta_o<0$ from Eq. (1). Obviously, the negative sign of the normal contact force is not consistent with the friction contact problem, implying that the steady-sliding equilibrium does not exist under this condition.

Suppose the system has compliances which are modeled by a spring inclined by θ_o and a lateral spring in the sliding direction as shown in Fig. 1(b). If the mass is assumed to slightly move only in the x-direction, the resulting force acting on the mass can be found as the following:

$$\mathbf{F}_{\text{body}}=(F-k_2x)\mathbf{i}+(N-L)\mathbf{j}+\mathbf{F}_s, \tag{3}$$

where the reacting force $\mathbf{F}_s$ of the inclined spring becomes

$$\mathbf{F}_s=-kx\cos\theta_o(\cos\theta_o\mathbf{i}+\sin\theta_o\mathbf{j}). \tag{4}$$

For θ_o at equilibrium, the equation of motion for the dynamic model can be written as

$$m\ddot{x}+\{k(\cos^2\theta_o-\mu\cos\theta_o\sin\theta_o)+k_2\}x=\mu L, \tag{5}$$

where

$$\sum F_y=N-L-kx\cos\theta_o\sin\theta_o=0. \tag{6}$$

The friction coefficient μ is generally assumed to be a nonlinear function of the sliding velocity $V_{\text{rel}}=V-\dot{x}$. Linearizing this relation about $V_{\text{rel}}=V$ gives

$$\mu=\mu_o-\left.\frac{\partial\mu}{\partial V_{\text{rel}}}\right|_{\dot{x}=0}\dot{x}+O(\dot{x}^2). \tag{7}$$

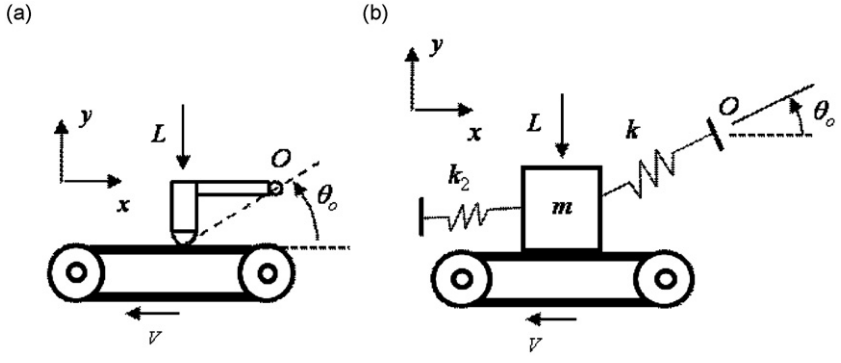

Fig. 1. Description of models, (a) static sprag model, (b) 1D dynamic sprag model.

By applying Eq. (7) to Eq. (5), the equation of motion takes the form of

$$m\ddot{x}+C_{\mu}L\dot{x}+(C_{\mu}k\cos\theta_o\sin\theta_o)\dot{x}x+\{k\cos^2\theta_o(1-\mu_o\tan\theta_o)+k_2\}x=\mu_oL, \tag{8}$$

where C_μ represents for the coefficient of friction-velocity slope defined by

$$C_{\mu}\equiv\left.\frac{\partial\mu}{\partial V_{\mathrm{rel}}}\right|_{\dot{u}=0}. \tag{9}$$

Note that the term $\dot{x}x$ provides a linear term as follows.

By using the dimensionless time $\tau=t\sqrt{k_2/m}$ and the coordinate transformation $x(t)=u(t)+x_o$, the linearized equation of motion becomes

$$u''+\frac{C_{\mu}L}{\sqrt{mk_2}}u'+\frac{C_{\mu}k\cos\theta_o\sin\theta_o}{\sqrt{mk_2}}x_ou'+\left\{\frac{k}{k_2}\cos^2\theta_o(1-\mu_o\tan\theta_o)+1\right\}u=0, \tag{10}$$

where $(\cdot)'$ denotes differentiation with respect to τ and the steady-sliding deformation x_o takes the form of

$$x_o=\frac{\mu_oL}{k\cos^2\theta_o(1-\mu_o\tan\theta_o)+k_2}. \tag{11}$$

For Spurr's model (k_2=0), $1-\mu_o\tan\theta_o=0$ is the sprag condition for an unbounded steady-sliding deformation. This geometric condition was considered the source of instability for the ensuing sprag-slip oscillations in this discussion. In this model for $k_2\neq0$, $\varepsilon k\cos^2\theta_o+k_2=0$ will be the modified sprag condition where

$$\varepsilon=1-\mu_o\tan\theta_o. \tag{12}$$

Finally, Eq. (10) is further simplified by introducing new parameters such that

$$u''+\beta\left(\frac{1+\delta}{1+\varepsilon\delta}\right)u'+(\varepsilon\delta+1)u=0, \tag{13}$$

where

$$\beta=\frac{C_{\mu}L}{\sqrt{mk_2}}, \tag{14}$$

$$\delta=\frac{k}{k_2}\cos^2\theta_o. \tag{15}$$

The parameter δ provides the contribution ratio of spring components to the lateral stiffness in the manner that δ can be increased by either a decrease in k_2 or a decrease in the angle θ_o. Here the sprag condition can be rewritten by using new parameters

$$1+\varepsilon\delta=0. \tag{16}$$

It should be noted that the sprag condition of Eq. (16) produces an infinite damping coefficient in the equation of motion of Eq. (13).

The normal contact force at steady-sliding can be found from Eqs. (6) and (11):

$$\frac{N}{L}=\frac{1+\delta}{1+\varepsilon\delta}. \tag{17}$$

For $1+\varepsilon\delta<0$, however, the normal contact force becomes negative, which breaks the frictional contact at the sliding surface as discussed earlier. Therefore, the condition for the sign change of the normal contact force and spragging ($1+\varepsilon\delta\leq0$) will not allow the steady-sliding state of the mass.

For the schematic interpretation (Fig. 2) for the sign change in normal contact force, the contact and total spring forces in terms of their direction angles are introduced as below

$$\mathbf{F}_c=F\mathbf{i}+N\mathbf{j}, \tag{18}$$

$$\mathbf{F}_T=-(k_2x+kx\cos^2\theta_o)\mathbf{i}-(kx\cos\theta_o\sin\theta_o)\mathbf{j}, \tag{19}$$

$$\tan\varphi=\frac{N}{F}=\frac{1}{\mu}, \tag{20}$$

$$\tan\eta=\frac{F_{Ty}}{F_{Tx}}=\frac{k\cos\theta_o\sin\theta_o}{k_2+k\cos^2\theta_o}. \tag{21}$$

When $\varphi>\eta$, the block can experience the steady-sliding as seen in Fig. 2(a). At $\varphi=\eta$, the forces $\mathbf{F}_c$ and $\mathbf{F}_T$ are aligned; the only way that the block can be in equilibrium with $L\neq0$ is to have the magnitude of both $\mathbf{F}_c$ and $\mathbf{F}_T$ equal to infinity. Note that when $\varphi=\eta$, $1+\varepsilon\delta=0$; that is, the sprag condition corresponds to the alignment of the total spring force vector with the contact force vector. When $\varphi<\eta$, the system cannot be in equilibrium since the vector sum of the three forces acting

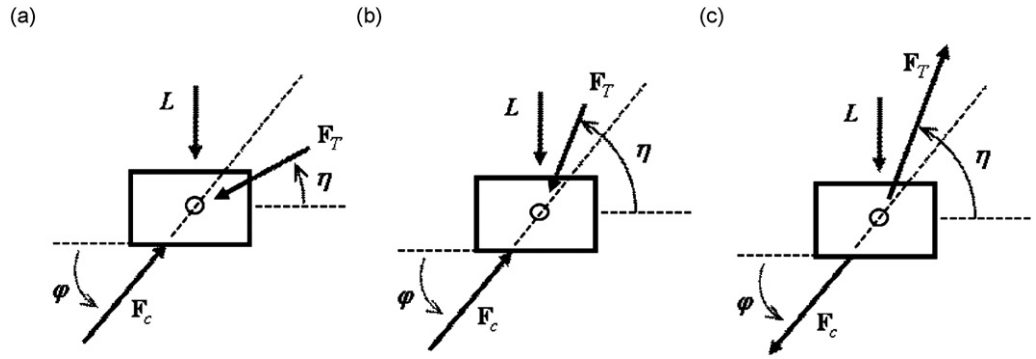

Fig. 2. Scheme for the existence of the equilibrium, (a) $\varphi > \eta$; equilibrium possible, (b) $\varphi < \eta$; equilibrium impossible, (c) $\boldsymbol{\varphi} < \eta$; equilibrium possible only if both F_c and F_T reverse sign.

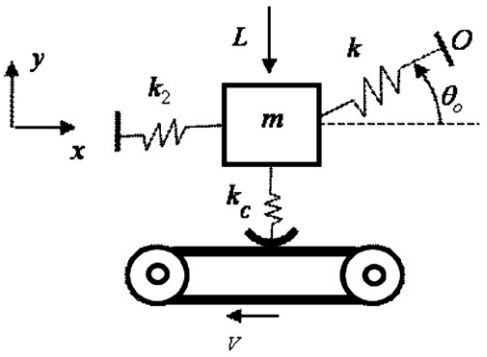

Fig. 3. 2D dynamic sprag model.

on the block cannot be zero as seen in Fig. 2(b). However, if the signs of $\mathbf{F}_c$ and $\mathbf{F}_T$ are reversed as in Fig. 2(c), the block can be in equilibrium. It points out that it is not only the sign of the normal contact force that can change, but the friction force and spring force must also change in sign. This is not consistent with the friction contact model. This discussion suggests that this sliding model is valid for only angles $\varphi > \eta$. Hoffmann and Gaul [15] have observed the same type of loss of the steady-sliding solution in a similar low-order model. Their interpretation of this condition is that the slider must lose contact with the belt under these conditions. This is a reasonable assumption. However, it is also possible that other compliances not included in these models could allow for steady-sliding solutions to exist in these regimes corresponding to classical spragging.

2.2. Two-dimensional sprag model

The dynamic sprag model is now modified by adding the contact stiffness k_c as shown in Fig. 3. This model in the previous literature [10,18] has been used for demonstrating the mode-coupling instability in the absence of spragging. For this reason, the existence of the steady-sliding equilibrium is investigated in terms of the coupling angle where its influence on the squeal oscillation due to mode-coupling is demonstrated at steady-sliding. In addition, the dynamic similarities and differences between the one- and two-dimensional models are provided here.

In the two-dimensional dynamic sprag model, the vertical motion is accounted for in the manner that the body force acting on the mass is described as

$$\mathbf{F}_{\text{body}} = -k_2 x\mathbf{i} - (k_c y + L)\mathbf{j} + \mathbf{F}_s, \tag{22}$$

where the inclined spring force is obtained by

$$\mathbf{F}_s = -k(x\cos\theta_o + y\sin\theta_o)(\cos\theta_o\,\mathbf{i} + \sin\theta_o\mathbf{j}), \tag{23}$$

Therefore, the equations of motion for the modified dynamic sprag model take the form:

$$m\ddot{x} + (k\cos^2\theta_o + k_2)x + k\sin\theta_o\cos\theta_o\, y = -\mu k_c y, \tag{24}$$

$$m\ddot{y} + k\sin\theta_o\cos\theta_o\, x + k\sin^2\theta_o\, y = -k_c y - L. \tag{25}$$

It is noted that Eq. (24) reduces to Eq. (5) if the contact spring force $k_c y$ is set equal to the normal contact force $-N$. Consequently, the choice of the dynamic sprag models of Figs. 1(b) and 3 is the matter of existence of vertical oscillations. Here the friction curve is also linearized in this model as in Eq. (7).

Similarly, the origin is shifted to zero by introducing the perturbations u and v from x_o and y_o, respectively, in such a manner that $x=x_o+u$ and $y=y_o+v$, where the steady-sliding deformations are obtained by

$$x_o = \frac{L(\mu_o k_c/\cos^2\theta + k\tan\theta_o)}{k\cdot k_c(1-\mu_o\tan\theta_o)+k_2(k_c/\cos^2\theta_o + k\tan^2\theta_o)}, \tag{26}$$

$$y_o = \frac{-L(k_2/\cos^2\theta_o + k)}{k\cdot k_c(1-\mu_o\tan\theta_o)+k_2(k_c/\cos^2\theta_o + k\tan^2\theta_o)}. \tag{27}$$

The sprag condition for this system becomes

$$k\cdot k_c(1-\mu_o\tan\theta_o)+k_2(k_c/\cos^2\theta_o + k\tan^2\theta_o)=0. \tag{28}$$

By using the dimensionless time $\tau = t\sqrt{k_2/m}$, the linearized equations of motion are written as

$$u'' - \frac{C_\mu k_c y_o}{\sqrt{mk_2}}u' + \left(\frac{k}{k_2}\cos^2\theta_o + 1\right)u + \left(\frac{k}{k_2}\sin\theta_o\cos\theta_o + \mu_o\frac{k_c}{k_2}\right)v = 0, \tag{29}$$

$$v'' + \frac{k}{k_2}\sin\theta_o\cos\theta_o u + \left(\frac{k}{k_2}\sin^2\theta_o + \frac{k_c}{k_2}\right)v = 0, \tag{30}$$

where $(\cdot)'$ denotes differentiation with respect to τ. Finally, the equations of motion are expressed as

$$u'' + \beta\left(\frac{1+\delta}{1+\varepsilon\delta+\gamma^{-1}\sin^2\theta_o}\right)u' + (1+\delta)u + \frac{1}{\sigma}(\sin\theta_o\cos\theta_o + \mu_o\gamma)v = 0, \tag{31}$$

$$v'' + \frac{1}{\sigma}\sin\theta_o\cos\theta_o u + \frac{1}{\sigma}(\sin^2\theta_o + \gamma)v = 0, \tag{32}$$

where

$$\sigma = \frac{k_2}{k}(>0). \tag{33}$$

$$\gamma = \frac{k_c}{k}(>0). \tag{34}$$

The sprag condition of Eq. (28) for this two degree-of-freedom model is rewritten as

$$1+\varepsilon\delta+\gamma^{-1}\sin^2\theta_o = 0. \tag{35}$$

Note that this sprag condition reduces to that of the single degree-of-freedom model (Eq. (16)) as $\gamma\to\infty$, as expected. This also provides an infinite damping coefficient, as seen in Eq. (31). This two-dimensional dynamic sprag model can be now used to describe the self-excited oscillations due to mode-coupling and negative friction-slope mechanisms and the sprag conditions. Here the normal contact force at steady-sliding can be found as well:

$$\frac{N}{L} = -\frac{k_c y_o}{L} = \frac{1+\delta}{1+\varepsilon\delta+\gamma^{-1}\sin^2\theta_o}, \tag{36}$$

where $1+\varepsilon\delta+\gamma^{-1}\sin^2\theta_o < 0$ should break the steady-sliding state due to the sign change of the normal contact force. Therefore, the sprag condition of the 2D dynamic sprag model will be the onset of the regime breaking the steady-sliding as well.

3. Analysis and results

As seen in the previous section, both the single- and two-degree-of-freedom models have parameter spaces for which the slider is seen to lift off the belt. It was concluded that in these spaces, steady-sliding is not possible within the constraints of these models. In this section, we will investigate the parameter spaces for which steady-sliding does exist. A perturbational eigenvalue analysis is presented to determine the stability of steady-sliding within these spaces. In addition, the resulting self-excited nonlinear responses where unstable steady-sliding exists are presented.

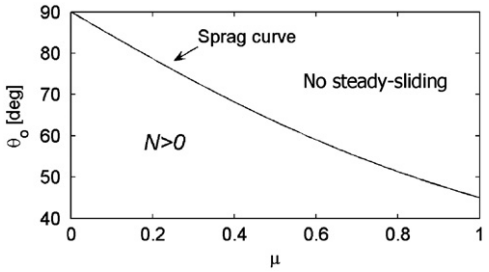

Fig. 4. Sprag curve of the static sprag model (the boundary of the no steady-sliding).

3.1. One-dimensional sprag model

From Eqs. (1), (17) and (36), it is concluded that the sprag condition defines the onset of the no steady-sliding. In the static sprag model (Fig. 1(a)), the inclined angle required for the no steady-sliding decreases as the friction coefficient increases (Fig. 4).

The analysis for the 1D dynamic sprag model (Fig. 1(b)) is provided as follows. First, the no steady-sliding and sprag conditions are obtained as the following case.

Case I. No steady-sliding

$$1+\varepsilon\delta \le 0. \tag{37}$$

The condition for the sign change in the normal contact force is equivalent to a negative stiffness of Eq. (13). Steady-sliding does not exist under this condition. Again, the sprag curve, $1+\varepsilon\delta=0$ becomes the border of the no steady-sliding.

In the case of the existence of the steady-sliding, parametric equilibrium stability is determined analytically. Substitution of $u=Ue^{\lambda t}$ into Eq. (13) produces the eigenvalue solutions of

$$\lambda_{1,2}=-\frac{\beta}{2}\left(\frac{1+\delta}{1+\varepsilon\delta}\right)\pm\frac{1}{2}\sqrt{\left(\frac{\beta(1+\delta)}{1+\varepsilon\delta}\right)^2-4(1+\varepsilon\delta)}, \tag{38}$$

subject to $1+\varepsilon\delta>0$ (condition for the existence of the steady-sliding).

For $\mathrm{Re}(\lambda)\neq 0$, this eigenvalue pair determines the stability of the local behavior of the steady-sliding in the nonlinear Eq. (5) according to Hartman–Grobman theorem [19]. Particularly, it should be noted that the sign of β and $1+\varepsilon\delta$ directly influence the equilibrium stability and the non-existence of steady-sliding. The following stability criteria are summarized as follows.

Case II. Source ($\mathrm{Im}(\lambda_{1,2})=0$ and $\lambda_1>\lambda_2>0$)

$$1+\varepsilon\delta>0. \tag{39}$$

and

$$\beta<-\frac{2(1+\varepsilon\delta)^{3/2}}{(1+\delta)^2}. \tag{40}$$

This condition can be met only by the negative slope of a friction-velocity curve. The source-type instability cannot retain oscillatory motions even with a positive stiffness in the sliding direction when an excessively large negative value of the damping coefficient is present.

Case III. Sink ($\mathrm{Im}(\lambda_{1,2})=0$ and $\lambda_2<\lambda_1<0$)

$$1+\varepsilon\delta>0, \tag{41}$$

and

$$\beta>\frac{2(1+\varepsilon\delta)^{3/2}}{(1+\delta)^2}. \tag{42}$$

The system parameters satisfying these parametric conditions will stabilize the steady-sliding. The condition related to system frequency (42) splits the stable region into sink and spiral-in type stabilities.

Case IV. Spiral-in ($\mathrm{Im}(\lambda_{1,2})\neq 0$ and $\mathrm{Re}(\lambda_1)<0$)

$$1+\varepsilon\delta>0, \tag{43}$$

and

$$0<\beta<\frac{2(1+\varepsilon\delta)^{3/2}}{(1+\delta)^2}, \tag{44}$$

where the system response near the steady-sliding will decay as damped oscillations.

Case V. Spiral-out ($\mathrm{Im}(\lambda_{1,2})\neq 0$ and $\mathrm{Re}(\lambda_1)>0$)

$$1+\varepsilon\delta>0, \tag{45}$$

and

$$-\frac{2(1+\varepsilon\delta)^{3/2}}{(1+\delta)^2}<\beta<0. \tag{46}$$

This flutter type instability produces the friction-induced vibration near the steady-sliding equilibrium in this dynamic sprag model. From the condition (46), it can be concluded that the spiral-out instability can be observed only for friction laws with a negative slope at the operating state.

For clarification, the stiffness ratio σ of the spring components is used in this analysis. In Fig. 5, the stability boundaries for the five cases above are illustrated, where the equilibrium stability cannot be defined on the regime of Case I. For $\sigma=0(k_2=0)$, Case V was introduced by Spurr's dynamic sprag model corresponding to the flutter instability produced by the negative friction slope ($\beta<0$). For $\sigma\neq 0(k_2\neq 0)$, the increase of negative friction slope can drop the fundamental frequency to zero by moving the steady-sliding from case V to II. From a practical point of view, the propensity of the flutter instability (Case V) can be the issue for a given negative value of β (negative friction-velocity slope). Geometric configuration influences on it in such a way that the regime of Case V can shrink near the boundary of Case I for $\varepsilon\leq 0$ and expand for $\varepsilon>0$.

Attention is paid to the sprag condition, $\varepsilon\delta+1=0$ as being a boundary of Case I (no steady-sliding) as shown in Fig. 5. Fig. 6 demonstrates the relationship between the range of stiffness values of $\sigma=k_2/k$ required for the appearance of the no steady-sliding, where the sprag curve of Fig. 6 represents the critical values of ε and σ satisfying the sprag condition. Note that for $\sigma<\sigma_c$ the sprag condition can be met. In this example of $\mu_o=0.7$, as σ goes to zero, the sprag angles are approximately 55° and 90°, where the steady-sliding equilibrium does not exist between 55° and 90°.

Fig. 7 illustrates the stability boundaries with the change of β. It implies that the negative friction slope, pre-normal load and the stiffness in the sliding direction change the dynamic characteristics around the steady-sliding. For example,

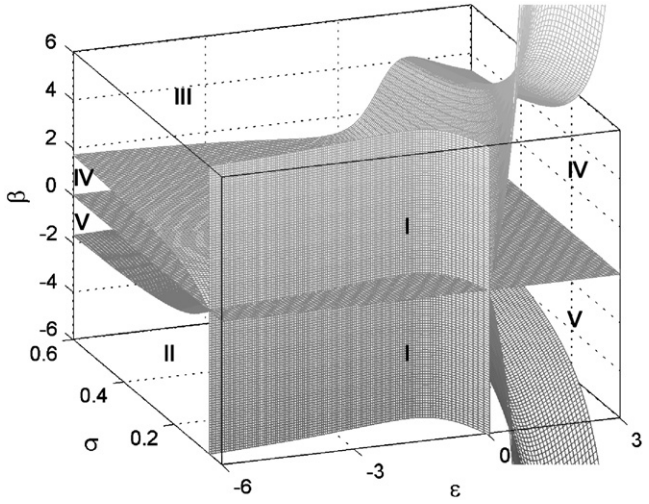

Fig. 5. Parametric stability for the 1D dynamic sprag model, I: no steady-sliding, II: source, III: sink, IV: spiral-in, V: spiral-out, $\mu_o=0.7$.

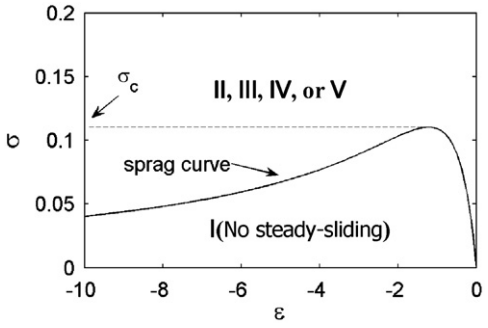

Fig. 6. Dynamic characteristics around sprag curve in the $\varepsilon-\sigma$ plot for the 1D dynamic sprag model, $\mu_o=0.7$.

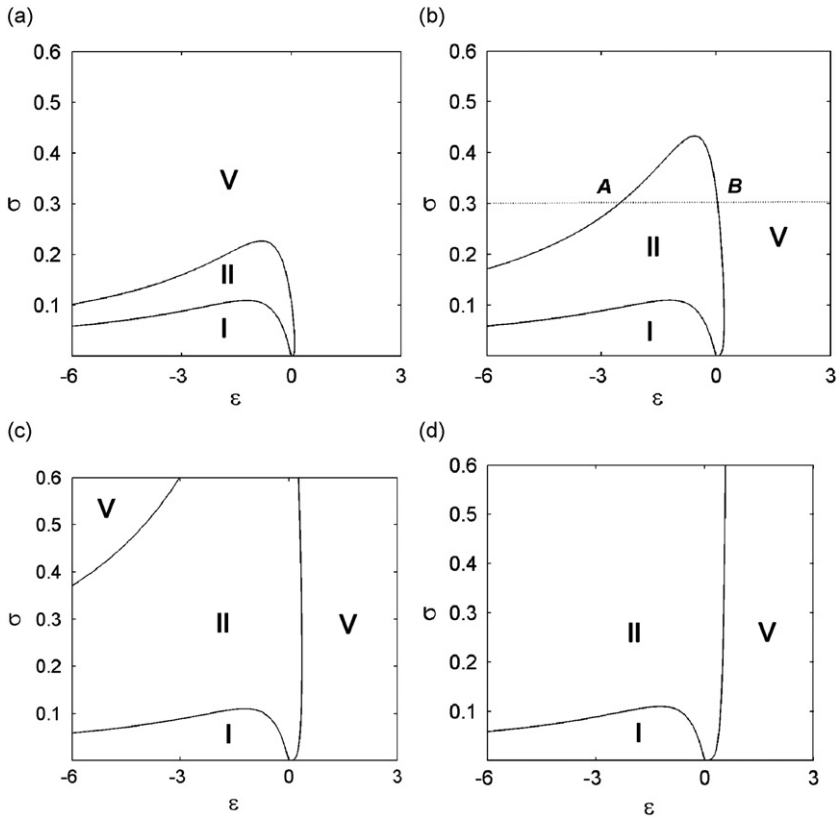

Fig. 7. Parametric stability on $\varepsilon-\sigma$ domain at, (a) $\beta=-0.5$, (b) $\beta=-1.0$, (c) $\beta=-1.5$, (d) $\beta=-2.0$, for the one-dimensional model.

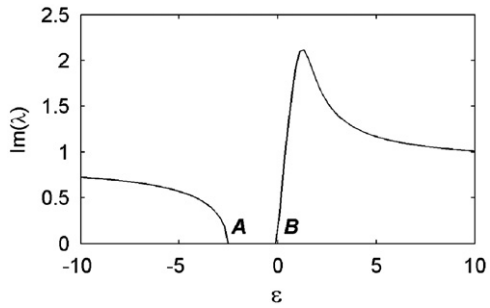

Fig. 8. Variation of imaginary part of the eigenvalue at $\beta=-1.0$ and $\sigma=0.3$ (on the region of II and V) for the one-dimensional model.

the regime of flutter instability (case V) disappears as the negative value of β is increased. Besides, it is known that the tribologic and geometric changes can alter the squeak frequencies [20]. For demonstrating this, Fig. 8 shows that the imaginary part of the eigenvalue drastically changes with respect to the sprag variable ε, where ε is the function of the tribologic and geometric factors such as the friction coefficient and the inclination angle. This sudden change in the system frequency is attributed to the shift between the types of equilibrium instability with respect to the variation of system parameters. It is shown in Fig. 7(b) and 8 that the boundaries of the instability type, ***A*** and ***B*** corresponds to the critical values for $\mathrm{Im}(\lambda)=0$.

3.2. Two-dimensional dynamic sprag model

Similarly, the parametric space for the existence of the steady-sliding is found first, where the dynamic characteristics of the two-dimensional system ((31)–(32)) are determined by $\mathrm{Re}(\lambda)$ and $\mathrm{Im}(\lambda)$.

Case I_{2D}. No steady-sliding

$$1+\varepsilon\delta+\gamma^{-1}\sin^2\theta_o \le 0, \tag{47}$$

which is equivalent to

$$-(1+\gamma+\sigma)+\sqrt{(1+\gamma-\sigma)^2+4\sigma(\sigma-\gamma\varepsilon)\delta} \ge 0. \tag{48}$$

In the parametric space except the above, the stability of the steady-sliding equilibrium for β=0 is determined by

$$\lambda = \pm\frac{1}{\sqrt{2\sigma}}\sqrt{-(1+\gamma+\sigma)\pm\sqrt{(1+\gamma-\sigma)^2+4\sigma(\sigma-\gamma\varepsilon)\delta}}, \tag{49}$$

subject to $1+\varepsilon\delta+\gamma^{-1}\sin^2\theta_o > 0$ (condition for the existence of the steady-sliding). From the Eq. (49), the stability of the steady-sliding can be summarized by the following.

Case II_{2D}. Marginal oscillation ($\mathrm{Im}(\lambda) > 0$ and $\mathrm{Re}(\lambda) = 0$)

$$(1+\gamma-\sigma)^2+4\sigma(\sigma-\gamma\varepsilon)\delta > 0, \tag{50}$$

and

$$1+\varepsilon\delta+\gamma^{-1}\sin^2\theta_o > 0. \tag{51}$$

Case III_{2D}. Spiral-out ($\mathrm{Im}(\lambda) > 0$ and at least one $\mathrm{Re}(\lambda) > 0$)

$$(1+\gamma-\sigma)^2+4\sigma(\sigma-\gamma\varepsilon)\delta < 0. \tag{52}$$

Particularly, the flutter instability of Case III_{2D} does not contain the negative friction-slope parameter β, but rather it is related to the mode-coupling instability. It should be noted that the mode-coupling instability can be generated only when $\varepsilon > 0$ (from $\sigma-\gamma\varepsilon < 0$) that corresponds to $90^\circ < \theta_o < 180^\circ$ or $0^\circ < \theta_o < \theta_{\varepsilon=0}$.

Figs. 9 and 10 illustrate the boundaries of the existence and stability of the steady-sliding equilibrium. These figures show some interesting relationships among the three stiffnesses, inclination angle and friction coefficient. When the contact stiffness γ is decreased, the region in the $\sigma-\varepsilon$ plane corresponding to the onset of squeal is significantly decreased. Alternately, there are no values of ε (i.e. μ_o and θ_o) for which squeal can occur for small k_c. As γ increases above a certain value, the combination of ε and σ required for squeal is specified in such a way that $\varepsilon > 0$ and $\sigma^c_{\min} < \sigma < \sigma^c_{\max}$. Therefore, the regime of mode-coupling instability relies on the combination of stiffness ratios and sprag parameter ε. Note that the no steady-sliding can arise only with a negative value of ε and small $\sigma(>0)$. In addition, Fig. 11 shows that the imaginary part of the eigenvalues of the two-dimensional system can vary drastically at certain conditions similar to that of the one-dimensional model.

Here the sprag curve is determined in this two degree-of-freedom model as well. It should be highlighted that the sprag curve becomes the onset of the no steady-sliding as seen in the one-dimensional system. Fig. 12 illustrates that the sprag curve approaches to that of Fig. 6 for the increase of the contact stiffness γ as expected in Eq. (35). When γ is decreased, the value of σ required for the sprag condition decreases. Alternately, the softer contact stiffness requires the less lateral stiffness for the onset of spragging.

The nonzero damping is known to alter the eigenvalue loci in terms of the negative damping and the difference between the damping coefficients of the mode-pair [8]. Fig. 13 illustrates how nonzero damping can influence the equilibrium instability by changing the real and imaginary parts of the eigenpair.

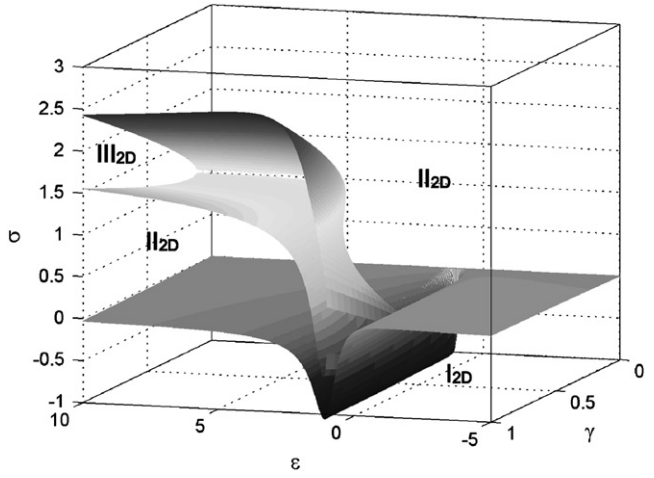

Fig. 9. Parametric stability, I_{2D}: no steady-sliding, II_{2D}: marginally stable, III_{2D}: spiral out (mode-coupling), μ_o=0.7 for two-dimensional model.

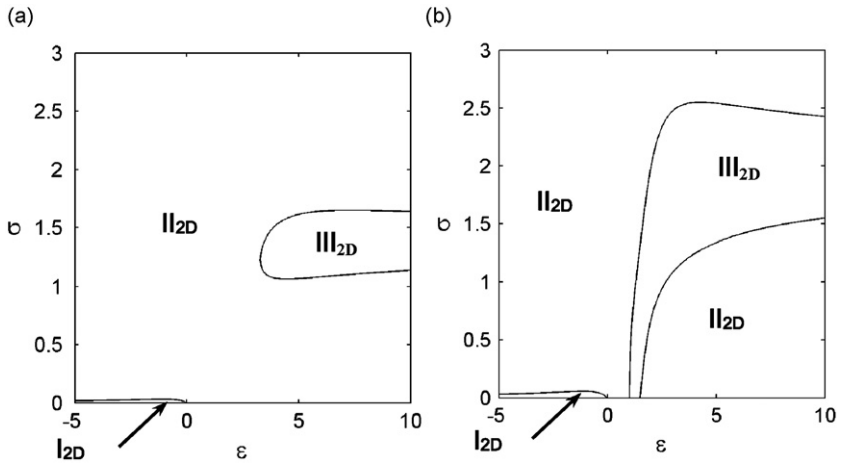

Fig. 10. Stability boundary on $\varepsilon-\sigma$ domain at, (a) γ=0.4, (b) γ=1.0 for two-dimensional model.

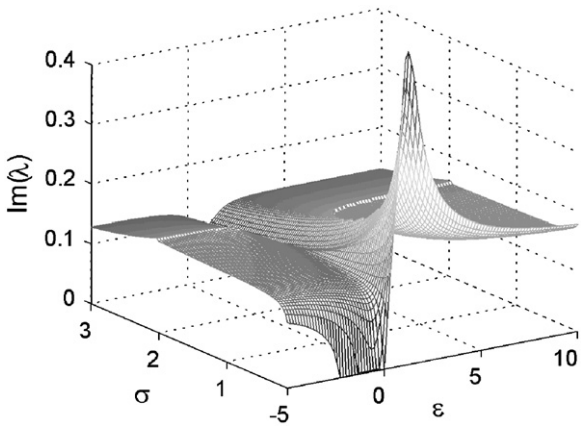

Fig. 11. The higher imaginary part of the mode pair with respect to ε and $\sigma(>0.1)$ at γ=1.0 (on the region of II_{2D} and III_{2D}) for two-dimensional model.

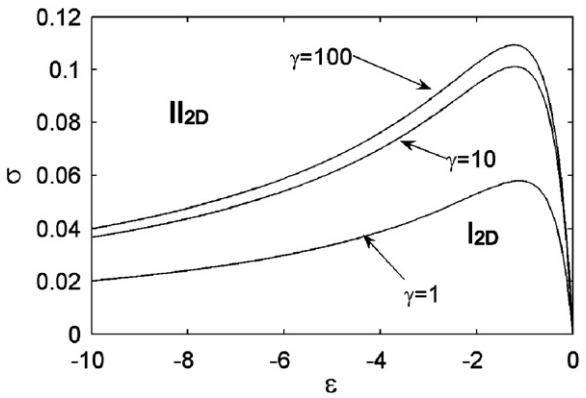

Fig. 12. Sprag curve for the two dimensional model, μ_o=0.7 for two-dimensional model.

3.3. Examples of nonlinear behavior

It has been observed that the dynamic behavior under the loss of steady-sliding solutions cannot be determined in the present models. Instead, nonlinear response away from the sprag regime will be illustrated here. First of all, the oscillations under the unstable steady-sliding equilibrium are demonstrated. The following friction curve is used in the original

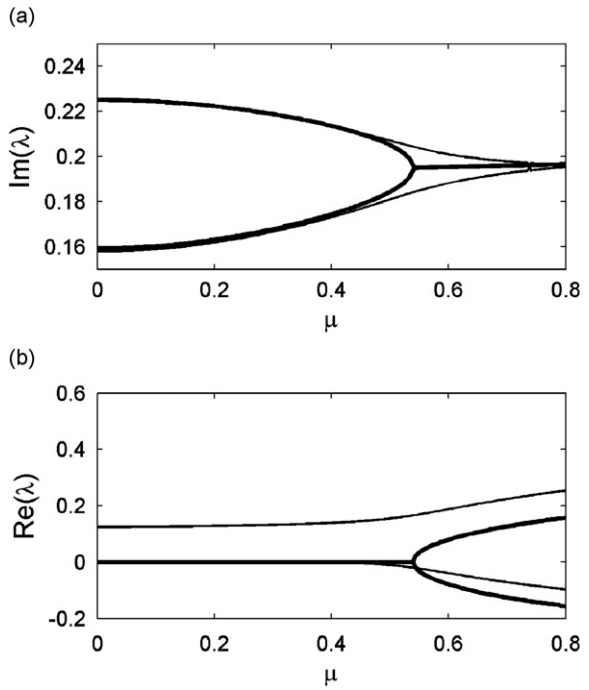

Fig. 13. The eigenvalue loci with respect to μ at $(\varepsilon,\sigma,\gamma)$=(1.8,1,1), (a) imaginary part, (b) real part, thick line: β=0, thin line: $\beta=-1$ for two-dimensional model.

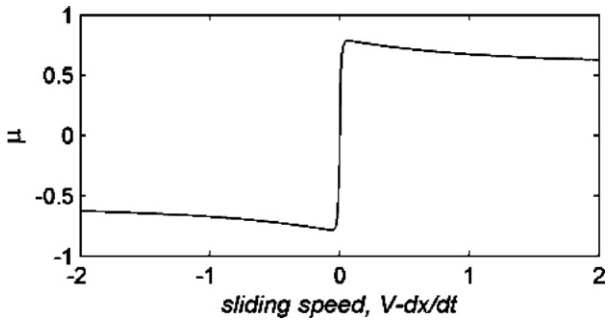

Fig. 14. Friction curve with respect to sliding speed.

equation of motion (5) ([9]):

$$\mu = \mathrm{sgn}(V-\dot{x})(1-e^{-\alpha|V-\dot{x}|})\{\mu_k-(\mu_k-\mu_s)e^{-\beta|V-\dot{x}|}\}, \tag{53}$$

where V is a belt speed and $(\mu_k,\mu_s,\alpha,\beta)$ are control parameters of the friction coefficient. An example of the friction law of Eq. (53) with a negative friction-velocity slope is illustrated in Fig. 14. On the basis of the stability boundaries from linear analysis shown in Fig. 5, the system parameters are chosen for demonstrating the nonlinear behavior of Case V. Fig. 15 shows how the stick-slip limit cycle motion is formed around the unstable steady-sliding equilibrium (Case V).

One type of divergence instability in the one-dimensional sliding system was a source type (Case II) which arises from an excessively negative damping coefficient. Due to the positivity of system stiffness in the sliding direction, the nonlinear response would eventually take a limit cycle stick-slip oscillation as illustrated in Fig. 16. The corresponding system frequency can be changed by a variation of a sprag parameter as shown in Fig. 17.

4. Conclusions and discussion

The single degree-of-freedom oscillator with an inclined spring has been developed as representing a sprag parameter in the system. From the analytical eigensolutions, it has been found that the sprag condition becomes the onset of the

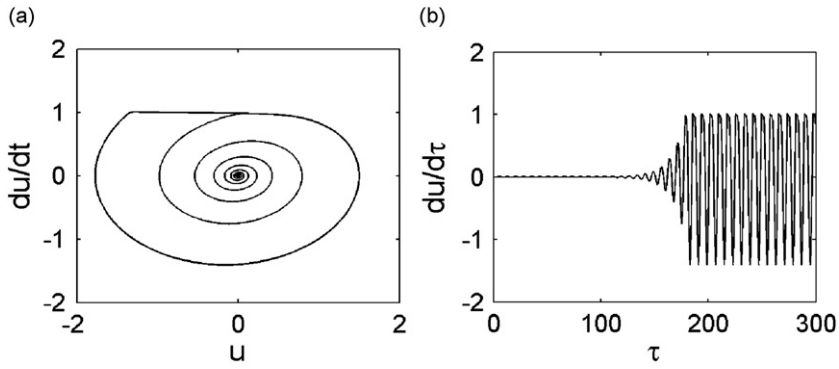

Fig. 15. The time history of criterion ④ at (μ_o, β,σ)=(0.7 – 0.1,0.3), (a) phase plane, (b) velocity, for the one-dimensional model.

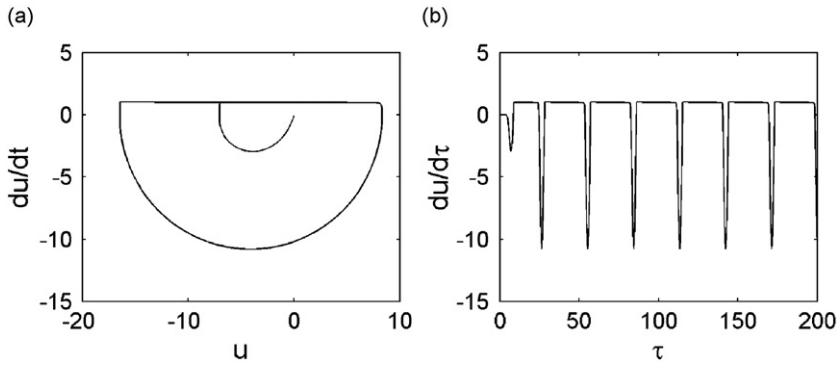

Fig. 16. The time history of criterion ③ at (μ_o, β,σ)=(0.7 – 2.0,0.3), (a) phase plane, (b) velocity, for the one-dimensional model.

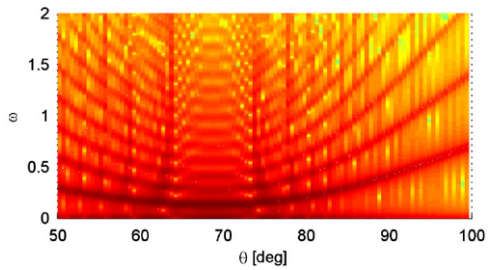

Fig. 17. Spectrogram at (μ_o, β,σ)=(0.7 – 2.0,0.3) for the one-dimensional model.

non-existence of a steady-sliding state. The negative damping induced by the negative friction-slope is essential for the generation of dynamic instability and becomes infinite under the sprag condition. Also, the vibration frequency is shown to change drastically along with the variation of sprag parameter.

In the two degree-of-freedom system, the sprag condition and the dynamic coupling between two modes have been addressed. The sprag condition of the 2D sprag model is influenced by contact stiffness, where it approaches to that of the 1D sprag model as the contact stiffness increases. It is found that the mode-coupling instability occurs only under a certain range of the sprag parameter as described by the mode-merging characteristics. This tendency is altered by the nonzero system damping. The frequency variation with respect to sprag parameter appears as well.

Most of all, the sprag condition is found to be the onset of the no steady-sliding. This sprag condition can occur only when the stiffness in the sliding direction is much smaller than the one at the inclination angle. The sprag angle corresponding to the sprag condition may not be unique. The no steady-sliding exists between the sprag angles, where it corresponds to the negative stiffness in the sliding direction.

In the model using a nonlinear friction curve, it is shown that the steady-sliding equilibrium can undergo stick-slip limit cycle oscillation. For the non-existence of steady-sliding, however, realistic and consistent nonlinear models including nonlinear springs, impacts and nonlinear geometric changes should be included for the possible simulation of the sprag-slip oscillations.

References

[1] R.A. Ibrahim, Friction-induced vibration, chatter, squeal and chaos Part II: dynamics and modeling, *Appl. Mech. Rev. ASME* 47 (1994) 227–253.
[2] C.A. Brockley, P.L. Ko, Quasi-harmonic friction-induced vibration, *J. Lubri. Tech. Trans. ASME* 89 (1970) 550–556.
[3] K. Popp, P. Stelter, Stick-slip vibrations and chaos, *Proc. R. Soc. London A* 332 (1990) 89–105.
[4] R.I. Leine, D.H.V. Campen, A.D. Kraker, L.V. Steen, Stick-slip vibrations induced by alternate friction models, *Nonlinear Dyn.* 16 (1998) 41–54.
[5] J. Kang, C.M. Krousgrill, F. Sadeghi, Dynamic instability of a thin plate with friction interface and its application to disc brake squeal, *J. Sound Vib.* 316 (2008) 164–179.
[6] J. Kang, C.M. Krousgrill, F. Sadeghi, Analytical formulation of mode-coupling instability in disc-pad coupled system, *Int. J. Mech. Sci.* 51 (2009) 52–63.
[7] J. Kang, C.M. Krousgrill, F. Sadeghi, Wave pattern motion and stick-slip limit cycle oscillation of a squealing disc, *J. Sound Vib.* 325 (2009) 552–564.
[8] J. Kang, C.M. Krousgrill, F. Sadeghi, Comprehensive stability analysis of disc brake vibrations including gyroscopic, negative friction slope and mode-coupling mechanisms, *J. Sound Vib.* 324 (2009) 387–407.
[9] J. Kang, C.M. Krousgrill, F. Sadeghi, Oscillation pattern of stick-slip vibrations, *Int. J. Nonlinear Mech.* 44 (2009) 820–828.
[10] J. Kang, Parametric study on friction-induced coupled oscillator, *Proc. IMechE, Part C: J. Mech. Eng. Sci.* 222 (2008) 1381–1387.
[11] R.T. Spurr, A theory of brake squeal, *Proceedings of Automotive Division, Institution Mechanical Engineers* (*AD*) Vol. 1, 1961, pp. 33–40.
[12] R.P. Jarvis, B. Mills, Vibrations induced by friction, *Proc. Inst. of Mech. Eng.* 178 (32) (1963) 847–857.
[13] S.W.E. Earles, C. Lee, Instabilities arising from the frictional interaction of a pin-disk system resulting in noise generation, *Trans. ASME, J. Eng. Ind.* 98 (1) (1976) 81–86.
[14] H. Keitzel, N. Hoffmann, Influence of the contact model on the onset of sprag-slip, *PAMM. Proc. Appl. Math. Mech.* 6 (2006) 311–312.
[15] N. Hoffmann, L. Gaul, A sufficient criterion for the onset of sprag-slip oscillations, *Arch. Appl. Mech.* 73 (2004) 650–660.
[16] M. Painleve, Sur les Lois du Frottement de Glissement, *Comptes Rendus de l'Academie des Scienc* 121 (1895) 112–115.
[17] D.E. Stewart, Rigid-body dynamics with friction and impact, *Soc. Ind. Appl. Math.* 42 (1) (2000) 3–39.
[18] N. Hoffmann, M. Fischer, R. Allgaier, L. Gaul, A minimal model for studying properties of the mode-coupling type instability in friction induced oscillations, *Mech. Res. Commun.* 29 (2002) 197–205.
[19] P. Hartmann, A lemma in the theory of structural stability of differential equations, *Proc. A. M. S.* 14 (1963) 568–573.
[20] B.L. Stoimenov, S. Maruyama, K. Adashi, K. Kato, The roughness effect on the frequency of frictional sound, *Tribol. Int.* 40 (2007) 659–664.